IET Radar, Sonar & Navigation

Research Article

IET Journals
The Institution of Engineering and Technology

Pietra index based processor for a heterogeneous Pareto background

ISSN 1751-8784
Received on 6th December 2018
Revised 17th March 2019
Accepted on 25th March 2019
E-First on 30th April 2019
doi: 10.1049/iet-rsn.2018.5608
www.ietdl.org

Ali Mehanaoui[1,2], Toufik Laroussi[1,2] ✉, Amar Mezache[2,3]

[1]*Département d'Electronique, Université des Frères Mentouri, Constantine 25000, Constantine, Algeria*
[2]*Laboratoire Signaux et Systèmes de Communication, 'SISCOM', Constantine, Algeria*
[3]*Département d'Electronique, Université Mohamed Boudiaf, M'sila 28000, Algeria*
✉ *E-mail: toufik_laroussi@yahoo.fr*

Abstract: This study addresses the problem of automatic target detection in a heterogeneous Pareto background. To achieve this, the Pietra index based and constant false alarm rate processor (CFAR) is conceived. Specifically, assuming a non-stationary Pareto background with the presence or not of any clutter edge or interfering targets, the Pietra index and the log geometric mean ratio statistic tests are concomitantly used to allow the proposed processor to switch dynamically to the appropriate detector; i.e. the geometric mean-CFAR, the greatest of-CFAR or the trimmed mean-CFAR, where all of these detectors assume a priori unknown scale parameter. That is, according to the outcomes of the Window Selection Probability, the background level is systematically estimated through the preselected detector. The detection performances of the proposed processor are assessed, via Monte Carlo simulations, in multiple target and clutter edge situations.

1 Introduction

As it is well-known, a good knowledge of the background model in which targets of interest may be embedded is beneficial to automatic target detection; which highly depends on the background's statistics. In order to reduce this sensitivity, while keeping constant the desired probability of false alarm, adaptive thresholding techniques have been used for decades [1, 2]. Constant false alarm rate (CFAR) detectors have been widely developed to deal with several detection schemes; however, a traditional detector is designed to treat only one kind of a situation. That is why, in real life applications, we often look for a robust processor to cope with all kinds of heterogeneities of the background under investigation.

The first works on radar detection show that CFAR detectors have been proposed to generally cope with a Gaussian background [3–7], which can be either homogeneous or heterogeneous. Whereas for homogeneous clutter, researchers look for optimal detectors, for heterogeneous clutter, they make do with suboptimal detectors. Heterogeneities may appear as an extended clutter edge or unwanted interfering targets. For instance, while some CFAR detectors rely upon automatic censoring algorithms to discard any number of unknown interfering targets and/or any unknown clutter edge position [4, 8], others make use of test statistics based on an irregularity index or the test cell information to select or build the prevailing CFAR detectors [9–14]. In this paper, we only focus on the second kind of detectors. For instance, Smith and Varshney [9] proposed the variability index CFAR (VI-CFAR) processor for a Gaussian background. Based on the outcomes of a second-order statistic, namely the variability index (VI) and the mean ratio (MR) of either half of the reference window; this processor judiciously switches to the cell averaging-CFAR (CA-CFAR) detector [15], the smallest Of-CFAR (SO-CFAR) detector [16] or the greatest Of-CFAR (GO-CFAR) detector [17]. It is worth noting that the VI-CFAR processor exhibits low CFAR-Loss values when operating in a homogeneous background and enough robustness in multiple target or clutter edge situations. Always for a Gaussian clutter and multiple target situations, Hammoudi and Soltani [10] introduced the performance of the distributed improved VI-CFAR (IVI-CFAR) algorithm. Using the 'AND', 'OR' and 'MAJORITY' fusion rules, the IVI-CFAR may also switch to the order statistics CFAR (OS-CFAR) whenever the interfering targets are spread in both halves of the reference window. Later, based on ordered data variability (ODV), Farrouki and Barkat [11] proposed the automatic censored cell averaging (ACCA) CFAR detector, i.e. ACCA-ODV-CFAR detector, for non-homogeneous Gaussian backgrounds (capture effect). This detector does not require any prior knowledge of the background and uses the VI statistic to reject or accept the ordered cells under investigation. It is shown that the ACCA-ODV-CFAR detector has the same performance as the CA-CFAR detector in a homogeneous background and performs robustly in a non-homogeneous one. Based on the test cell information, Cao [12] developed the switching-CFAR (S-CFAR) detector, which does not require any rank ordering. This detector is shown to achieve a small CFAR loss when operating in a homogeneous background and a good robustness in the presence of interfering targets or clutter edge situations. The improved and the generalised versions of the S-CFAR detector, namely, the improved S-CFAR (IS-CFAR) and the generalised S-CFAR (GS-CFAR) detectors are suggested in [13, 14], respectively.

With the advent of high resolution radars, the Gaussian distribution became no more suitable for radar clutter modelling. Non-Gaussian backgrounds such as log-normal, Weibull, K and Pareto, have then led to the development of new genres of CFAR detectors [18–20]. Automatic censoring for non-Gaussian background was introduced in [21–23]. Almarshad *et al.* [21] proposed the forward automatic censored cell averaging detector (F-ACCAD) CFAR for a lognormal clutter and multiple target situations. This detector uses ranked transformed normal samples to censor automatically the highest unwanted cells. The censoring and the detection algorithms are based on a biparametric linear threshold for which the parameters of the normal distribution are estimated using a simple linear approach. In [22], they considered the forward/backward automatic censoring order statistics detectors (F/B-ACOSD) CFAR by use of the Weber–Haykin adaptive threshold introduced in [23]. Recently, Chabbi *et al.* [24] introduced the dual automatic censoring best linear unbiased (DACBLU-CFCAR) detector in Weibull clutter, when both clutter edge and interferences are present in the reference window. In this detector, the censoring and the detection algorithms rely upon the same biparametric linear threshold based on the BLU estimators (BLUEs) of the Gumbel parameters. In [25], assessing that the VI-based approach makes the VI-CFAR detector lose the CFAR property for a Pareto distributed clutter; Weinberg proposed a

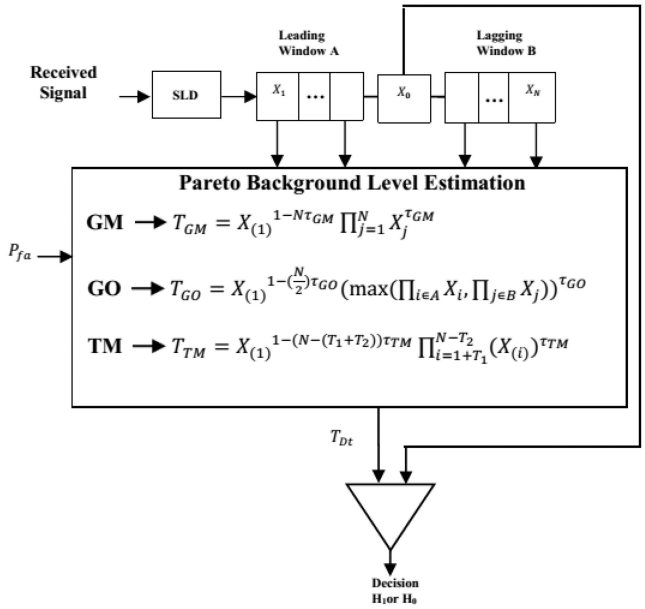

Fig. 1 *Block diagram of the Pareto CFAR detectors*

novel formulation of a generalised switching detector for any kind of the clutter model. Despite the interesting idea behind this detector, the switching procedure requires the a priori knowledge of the Pareto scale parameter. As an alternative, he tested its performance in a one parameter Lomax background, which happens to be an insufficient model for real data [26]. That is, the same author proposed an extended version of the work done in [25], based exclusively upon a geometric-mean detector with a full CFAR property.

In an attempt to use the VI as a heterogeneous Pareto background discriminator, Mehanaoui *et al.* [27] developed the enhanced VI-automatic selection and detection CFAR (EVI-ASD-CFAR) processor for multiple target situations. This approach is only useful for a priori known scale parameter, and therefore, for a Gaussian background. In effect, its switching procedure is used to dynamically select the suitable detector among the geometric mean-CFAR (GM-CFAR), the greatest Of-CFAR (GO-CFAR) and the trimmed mean-CFAR (TM-CFAR) detectors developed in [28]. In other words, the authors exploited the properties inherent to the duality between the Pareto and the exponential distributions. As the former detectors are not fully CFAR; i.e. the scale parameter should be a priori known, in this paper, we show how the Pietra index (PI) can be a good substitute for the VI in a heterogeneous non-Gaussian background. That is, in a Pareto context, we develop the PI-based CFAR (PI-CFAR) processor. In doing this, we analyse the performance of the proposed processor in the presence of interfering targets or clutter edge, in terms of the detectors developed by Weinberg [29, 30], which are known to attain the CFAR property for a priori unknown scale parameter. The remaining of the paper is organised as follows. In Section 2, we present an overview on the Pareto distribution along with its corresponding CFAR detectors. In Section 3, we describe the PI as a sensor of variability in a non-Gaussian background and develop in details the PI-CFAR processor. In Section 4, we conduct, by means of Monte Carlo simulations, a performance comparison of the proposed processor and the ones given in [29, 30]. In Section 5, we summarise and conclude the paper with the main results of our contribution.

2 Overview on CFAR detectors in a Pareto clutter

Studies on modelling X-band sea radar clutter have shown that the Pareto distribution constitutes the best fit to the received Ingara data [31]. The probability density function (PDF) of an observed random Pareto sample X in the intensity domain is given by [25–33]

$$f_X(x) = \frac{\alpha}{\beta}\left(\frac{\beta}{x}\right)^{\alpha+1}, \quad x \geq \beta \tag{1}$$

where $\alpha > 0$ and $\beta > 0$ are the shape and scale parameters, respectively.

Based on (1), with the assumption that β is a priori unknown, three CFAR detectors have been developed; namely, the GM-CFAR, GO-CFAR and TM-CFAR detectors [29, 30]. Their block diagram is depicted in Fig. 1. Let X_is, $i = 0, 1, 2, \ldots, N$ be the square law detector (SLD) matched filter output samples. They are assumed to be independent and identically distributed (IID) random variables drawn from the Pareto distribution whose PDF is given by (1). They are clocked and stored into a tapped delay line (TDL) of length $N + 1$, corresponding to the N reference cells and the cell under test (CUT) X_0. Their adaptive thresholds are denoted T_{GM_W}, where $W = A$, B or $A \circ B$ ('$\circ$' designates the concatenation operator), T_{GO} and T_{TM}, respectively. The constant coefficients τ_{GM_W}, τ_{GO} and τ_{TM} are sets such as the probability of false alarm (P_{fa}) remains equal to its preset value.

The probabilities of detection $P_{\mathrm{d}}^{\mathrm{Dt}}$ and false alarm $P_{\mathrm{fa}}^{\mathrm{Dt}}$ of the preselected detector are given, respectively, by [5]

$$P_{\mathrm{fa}}^{\mathrm{Dt}} = \int_0^{\infty} \Pr\left(X_0 > T_{\mathrm{Dt}} | H_0\right) f_{T_{\mathrm{Dt}}}(T_{\mathrm{Dt}}) \mathrm{d}T_{\mathrm{Dt}} \tag{2}$$

$$P_{\mathrm{d}}^{\mathrm{Dt}} = \int_0^{\infty} \Pr\left(X_0 > T_{\mathrm{Dt}} | H_1\right) f_{T_{\mathrm{Dt}}}(T_{\mathrm{Dt}}) \mathrm{d}T_{\mathrm{Dt}} \tag{3}$$

where Dt denotes either GM-, GO-, or TM-CFAR detector, $f_{T_{\mathrm{Dt}}}(T_{\mathrm{Dt}})$ the PDF of the corresponding adaptive threshold T_{Dt}, Pr the probability operator, H_0 the absence of a target, H_1 the presence of a target, $\Pr\left(X_0 > T_{\mathrm{Dt}} | H_0\right) = \int_{T_{\mathrm{Dt}}}^{\infty} f_{X_0|H_0}(x_0|H_0)\, \mathrm{d}x$ and $\Pr\left(X_0 > T_{\mathrm{Dt}} | H_1\right) = \int_{T_{\mathrm{Dt}}}^{\infty} f_{X_0|H_1)}(x_0|H_1) \mathrm{d}x$. Table 1 shows the expressions of the probabilities of detection and false alarm, $P_{\mathrm{d}}^{\mathrm{Dt}}$ and $P_{\mathrm{fa}}^{\mathrm{Dt}}$ of the three CFAR detectors. The detection performance of each of these detectors is assessed in a homogeneous and heterogeneous background in terms of the number of the training (reference) cells, the desired false alarm rate, the shape parameter and the H/V radar antenna polarisation [29, 30].

It is shown that the GM-, the GO- and the TM-CFAR detectors behave satisfactorily compared to the benchmark detector (fixed threshold) for a homogeneous background. However, for a heterogeneous clutter, the GM- and the GO-CFAR exhibit CFAR losses. That is, their detection performances are affected by the presence of the interfering targets. The TM-CFAR detector is known to censor the T_1 and T_2 upper and lower undesirable cells, respectively. For instance, $T_1 = 10\%$ and $T_2 = 20\%$ of N, preserve the robustness of the TM-CFAR detector; inducing a small CFAR loss which is due to the reduction of the number of training cells from N to $N - (T_1 + T_2)$ [32]. Its detection performance could be, however, optimised for higher values of N. Finally, it is also shown, that, for a clutter transition, the GO-CFAR detector controls fairly the probability of false alarm [5, 26].

3 PI-based CFAR processor

The PI is a valuable measure of statistical heterogeneity in socioeconomics and econophysics [34–36]. However, from a radar literature point of view, we observe that all of the above-cited works did not make any use of the PI. Hence, as stated earlier, based on this statistical background discriminator, we suggest the exploration of an alternative to the VI in a non-Gaussian background. The definition of the PI is given by [34]

$$\mathrm{PI} = \frac{1}{E[X]} \int_{E[X]}^{\infty} p_X(x) \mathrm{d}x \tag{4}$$

where $p_X(x \geq 0)$ is the survival function and $E[X]$ the mean of X. Equation (4) can be written as

$$\mathrm{PI} = \frac{1}{E[X]} E[\ \max\ (0, X - E[X])] \tag{5}$$

Proofs of (4) and (5) are given in [34, Appendix]. Note that the PI is an unbiased estimation of the deviation of the random variable X from its mean and normalised by its mean. It measures the largest excess of the data compared with the sample average. Graphically, it represents the maximum vertical deviation between the Lorenz curve and the egalitarian line [35]. It can also be written as

$$\mathrm{PI} = E\left[\ \max\ \left(0, \frac{X}{E[X]} - 1\right)\right] \tag{6}$$

or, it terms of the sample mean as

$$\mathrm{PI} = \frac{1}{N} \sum_{i=1}^{N}\ \max\ \left(0,\ \frac{X_i}{E[X]} - 1\right) \tag{7}$$

Recall that the VI is a second-order statistic which uses the variance to mean ratio. It represents a symmetric measurement for the irregularity of the random variable X around its mean. It is given by [9]

$$\mathrm{VI} = 1 + \frac{\hat{\sigma}^2}{\hat{\mu}^2} \tag{8}$$

where $\hat{\sigma}^2$ and $\hat{\mu}$ are, respectively, the estimated variance and mean of X. The VI is a measure of the statistical heterogeneity suited for a Gaussian background with symmetric unimodal PDF. Practically, the VI statistic introduced in [9], operates mainly in an exponentially distributed background and is shown to handle heterogeneity discrimination in merely the Gaussian clutter. The main limitation of the VI is its incapability to handle skewness and heavy-tailed behaviours of the Pareto distribution [25]. Furthermore, the variance, therefore the VI, for a Pareto distribution, does not exist for values of the shape parameter $\alpha \leq 2$. The *PI* statistics described in (4)–(6) is an asymmetric exceedance measurement of the random variable over its mean, inherent to a non-Gaussian background with skewed or heavy-tailed probability distributions. Here, in order to assess data variability, the *PI* is tested on the Pareto distribution given by (1). The results are shown in Section 3.

The estimation of the background level, in which the target of interest is embedded, is an essential task in target detection. Moreover, the estimator as well as its respective used number of samples affect the accuracy of the unknown background level estimation. The PI-CFAR processor is an automatic target detector which copes with the background vicissitudes. In order to select the correct background level estimation, the processor needs decisive information about the background nature. For this purpose, the PI and the Log Geometric Mean Ratio (LGMR) statistics, whose expressions are given below, are calculated and used in a switching logic. These latter allow the processor to tell whether the reference cells constitute a homogeneous set; in which case, the appropriate detector is preselected. This is accomplished through the use of two statistical tests on the PI and the LGMR. In this way, any irregularities in the background profile, i.e. the presence of a clutter edge or multiple target situations, are detected. In doing this, the reference window is first divided into two finite sub-sets of $N/2$ cells, namely, the leading (A) and the lagging (B) sub-windows. Then, the variability of each set is tested separately, and their respective means are calculated and compared. That is, as long as the calculated PI is below a certain threshold, the background is likely to be homogeneous. In other words, depending on the situation at hand, the switching logic selects automatically the desired detector; namely, the GM-, GO- or TM-CFAR.

Fig. 2 illustrates the block diagram of the proposed processor. It is mainly based on the set of CFAR detectors introduced in Section 2, in which the detector selection is governed by the statistical tests performed on the PI and the LGMR. Note that when both reference sub-windows include interfering targets, the X_is can also be rank-ordered to get the $X_{(i)}$, $i = 1, \ldots, N$, to be eventually treated by the TM-CFAR detector [30, 37].

The PI-CFAR processor decides, therefore, whether a homogeneous background exists, through the following hypothesis tests, involving the PI and the LGMR, as follows:

$$\mathrm{PI} \underset{\mathrm{hH}}{\overset{\mathrm{nhH}}{\gtrless}} \mathrm{TPI} \tag{9}$$

where TPI (Threshold PI) is a discriminating threshold chosen to ensure a low probability of error, the nhH hypothesis refers to a non-homogeneous background, i.e. the samples $X_1, X_2, \ldots, X_N$ correspond to the presence of a clutter edge or interferences, and the hH hypothesis to a homogeneous background. Now, let α_0 be the probability of making an erroneous decision upon the hypothesis test given by (9). It is defined as

$$\alpha_0 = \Pr\ (\mathrm{PI} > \mathrm{TPI} \,|\, \mathrm{hH}) \tag{10}$$

Table 1 Detectors in a Pareto background with a priori unknown scale parameter [29, 30]

Detector (Dt)	$P_{\mathrm{fa}}^{\mathrm{Dt}}$	$P_{\mathrm{d}}^{\mathrm{Dt}}$
GM-FAR	$P_{\mathrm{fa}}^{\mathrm{GM}} = \frac{N}{N+1}(1+\tau)^{-(N-1)}$	$P_{\mathrm{d}}^{\mathrm{GM}} = \Pr\left(\log\left(\frac{X_0}{X_{(1)}}\right) > \tau_{\mathrm{GM}} \sum_{j=1}^{N} \log\left(\frac{X_j}{X_{(1)}}\right) \middle| H_1\right)$
TM-CFAR	$P_{\mathrm{fa}}^{\mathrm{TM}} = \frac{N}{N+1} \prod_{j=1}^{N-T_1-T_2} M_{v_j}(\tau)$, where $M_{v_1}(\tau) = \frac{(N-1)!}{(T_1-1)!(N-T_1-1)!(N-T_1-T_2)!} \times \sum_{j=0}^{T1-1} \frac{\binom{T_1-1}{j}(-1)^{T_1-1-j}}{((N-1-j)/(N-T_1-T_2))+\tau}$ and $M_{v_j}(\tau) = \frac{(N-T_1-j+1)/(N-T_1-T_2-j+1)}{((N-T1-j+1)/(N-T1-T2-j+1))+\tau}$, for $2 \leq j \leq N-T_1-T_2$	$P_{\mathrm{d}}^{\mathrm{TM}} = \Pr\left(\log\left(\frac{X_0}{X_{(1)}}\right) > \tau_{\mathrm{TM}} \sum_{j=T_1+1}^{N-T_2} \log\left(\frac{X_j}{X_{(1)}}\right) \middle| H_1\right)$
GO-CFAR	$P_{\mathrm{fa}}^{\mathrm{GO}} = \frac{2N}{N+2}\left((1+\tau)^{-N/2} - \sum_{k=0}^{(N/2)-2} \binom{\frac{N}{2}+j-1}{j} (2+\tau)^{-((N/2)+j)}\right)$	$P_{\mathrm{d}}^{\mathrm{GO}} = \Pr\left(\log\left(\frac{X_0}{X_{(1)}}\right) > \tau_{\mathrm{GO}} \max\left(\sum_{j=1}^{N/2} \log\left(\frac{X_j}{X_{(1)}}\right), \sum_{j=(N/2)+1}^{N} \log\left(\frac{X_j}{X_{(1)}}\right)\right) \middle| H_1\right)$

Practically, to detect an effective change in the background, α_0 must be as small as possible and limited to the order of magnitude of the desired P_{fa}.

Let GMR be the ratio of the geometric means of the leading and the lagging windows, respectively. It is defined as

$$\text{GMR} = \frac{\text{GM}_{E[X_A]}}{\text{GM}_{E[X_B]}} \tag{11}$$

That is

$$\text{GMR} = \frac{\left(\prod_{i=1}^{N/2} X_i\right)^{2/N}}{\left(\prod_{i=(N/2)+1}^{N} X_i\right)^{2/N}} \tag{12}$$

Since the logarithm is a monotonically increasing function, taking the logarithm of (12), yields

$$\text{LGMR} = \log(\text{GMR}) = \frac{2}{N}\log\frac{\left(\prod_{i=1}^{N/2} X_i\right)}{\left(\prod_{i=(N/2)+1}^{N} X_i\right)} \tag{13}$$

or,

$$\text{LGMR} = \frac{2}{N}\left[\sum_{i=1}^{N/2}\log X_i - \sum_{i=(N/2)+1}^{N}\log X_i\right] \tag{14}$$

The hypothesis test on the LGMR is then given by

$$\begin{cases} \text{TMR}^{-1} \le \text{LGMR} \le \text{TMR}, & \text{same means} \\ \text{LGMR} < \text{TMR}^{-1} \text{ or LGMR} > \text{TMR}, & \text{otherwise} \end{cases} \tag{15}$$

The corresponding probability of error β_0 made upon the hypothesis test given by (15), is

$$\beta_0 = 1 - \Pr\left(\text{TMR}^{-1} \le \text{LGMR} \le \text{TMR} \,|\, \text{hH}\right) \tag{16}$$

where TMR (Threshold MR) is also a discriminating threshold chosen to ensure a low probability of error. In a clutter edge situation, β_0 controls the switching between the GO- and the GM-CFAR and vice versa. In a homogeneous background, values of TPI and TMR are chosen to ensure low probabilities of making erroneous decisions upon (9) and (15). As shown in Figs. 3 and 4, a trade-off is made, by simulation, to determine graphically the threshold values of α_0 and β_0, respectively. Note that a successful selection, which would make the processor sensitive to the background variations, is closely related to the values of these thresholds which must be neither too small nor too large. Finally, it is important to notice that (10) and (16) assume fixed thresholds TPI and TMR, respectively. At this, stage, we still lack of a solution to their adaptive issue.

The switching strategy is based on the selection logic of the PI-CFAR processor operating in a Pareto background. In doing so, we propose a procedure which deals with the inhomogeneities commonly encountered in automatic radar detection; namely, the presence of multiple targets or the presence of a clutter transition within the reference window. All possible situations, which are governed by the hypothesis tests on the PI and the LGMR, are summarised in Table 2.

Explicitly, depending on the problem at hand, the PI-CFAR processor selects the appropriate CFAR detector according to the results provided by the switching logic of this table. That is, each of the five rows corresponds to a situation that may be met in a real-world application. First, when the two reference sub-windows are homogeneous, i.e. $\text{PI}_A < \text{TPI}$ and $\text{PI}_B < \text{TPI}$, and there is no clutter edge, i.e. LGMR < TMR; therefore, the PI-CFAR processor switches to the GM-CFAR detector; which leads to row 1. Note that this detector is applied to the entire reference window $A \circ B$. Second, if either one of the reference sub-window is non-homogeneous; i.e. $\text{PI}_A \ge \text{TPI}$ or $\text{PI}_B \ge \text{TPI}$, irrespective of the test on the means, two cases can be encountered; namely the presence of a

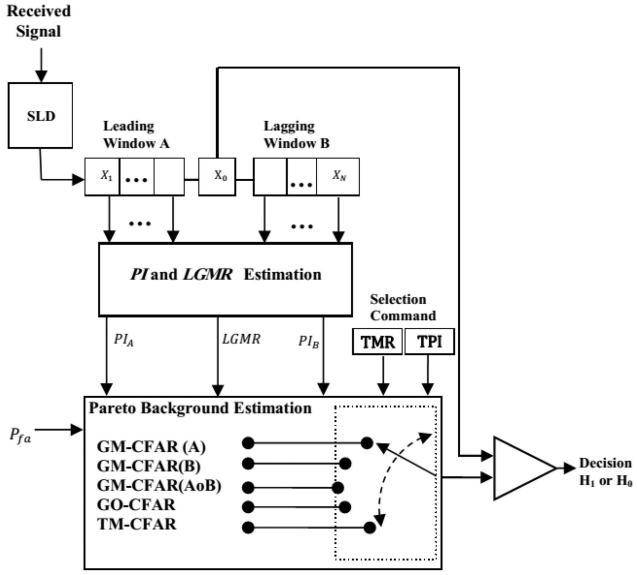

Fig. 2 *Block diagram of the PI-CFAR Processor*

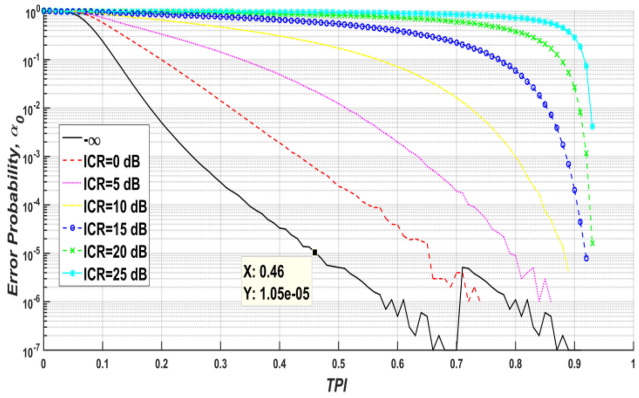

Fig. 3 *Simulated error probabilities* (α_0) *versus TPI in the presence of one interfering target; for* $N = 32$, $\alpha = 4.7241$, $P_{fa} = 10^{-5}$ *and ICR as a parameter*

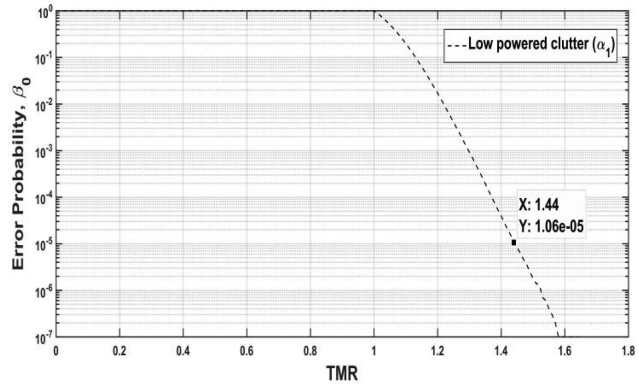

Fig. 4 *Simulated error probabilities* (β_0) *versus TMR; for* $N = 32$ *and* $\alpha = 4.7241$

clutter transition or the presence of interfering targets. In the former situation, the clutter edge could be in either side of the CUT, in such a case, the PI-CFAR processor chooses the homogeneous reference sub-window (A or B) and switches to the GM-CFAR detector with only $N/2$ cells; yielding row 3 or 4. Third, if the leading window and the CUT experience a high-power clutter, and the lagging window is immersed in a low-power clutter; thus both reference sub-windows have different means, i.e. LGMR > TMR but neither is non-homogeneous, i.e. $\text{PI}_A < \text{TPI}$ and $\text{PI}_B < \text{TPI}$. In such a case, the PI-CFAR processor sets its threshold according to the maximum of the leading and lagging sub-windows

Table 2 Selection logic

$PI_A \overset{nhH}{\geq} TPI$	$PI_B \overset{nhH}{\geq} TP?$	LGMR > TMR?	Adaptive threshold	Selected detector
no	no	no	$X_{(1)}^{1-N\tau_{GM}}\prod_{i=1}^{N}X_i^{\tau_{GM}}$	$GM_{A\circ B}$-CFAR
no	no	yes	$X_{(1)}^{1-(N/2)\tau_{GO}}(\max(\prod_{i\in A}X_i,\prod_{j\in B}X_j))^{\tau_{GO}}$	GO-CFAR
yes	no	do not care	$X_{(1)}^{1-(N/2)\tau_{GM}}\prod_{i=N/2}^{N}X_i^{\tau_{GM}}$	GM_B-CFAR
no	yes	do not care	$X_{(1)}^{1-(N/2)\tau_{GM}}\prod_{i=1}^{N/2}X_i^{\tau_{GM}}$	GM_A-CFAR
yes	yes	do not care	$X_{(1)}^{1-(N-(T_1+T_2))\tau_{TM}}\prod_{i=1+T_1}^{N-T_2}(X_{(i)})^{\tau_{TM}}$	TM-CFAR

geometric means, and thus switches to the GO-CFAR detector; which corresponds to row 2.

Before proceeding to the simulation section, take notice of the definitions of the respective probabilities of window selection A, B and $A\circ B$, noted PWS_A, PWS_B, and $PWS_{A\circ B}$

$$PWS_A = \Pr(T_{PI} = T_{GO|nhH} + T_{GM_A|nhH}) \quad (17)$$

$$PWS_B = \Pr(T_{PI} = T_{GM_B|nhH}) \quad (18)$$

$$PWS_{(AoB)} = \Pr(T_{PI} = T_{GM_{AoB}|hH} + T_{TM|nhH}) \quad (19)$$

where 'T_{PI}' designates the detection threshold of the PI-CFAR processor and '+' the logical 'OR' operator. Note that depending on the clutter heterogeneity, T_{PI} can be set equal to either T_{GM_W}, T_{GO} or T_{TM}.

Finally, a couple of events may also occur. First, the presence of one or more interfering targets in either reference sub-window; this case can be assimilated to the second situation in which the clutter edge is replaced by the interfering targets; that is row 3 or 4 is selected. Second, when both reference sub-windows contain interfering targets, i.e. $PI_A \geq TPI$ and $PI_B \geq TPI$, independently of the LGMR, the PI-CFAR processor switches to the TM-CFAR detector; which matches row 5.

4 Simulation results and discussion

In this section, we evaluate, through Monte Carlo simulations, the switching and detection performances of the PI-CFAR processor. To this effect, we deal with the following assumptions. A single-pulse detection, which corresponds to Swerling I and II models and $P_{fa} = 10^{-5}$. This means that 10^7 Monte Carlo trials; i.e. desired accuracy of 10%, are acceptable to obtain the thresholds [38, Appendix]. The interfering targets are primary target-like with the same interference to clutter ratio (ICR). The reference window size is $N = 32$, the upper and lower numbers of the censored cells are $T_1 = 3$ and $T_2 = 6$, respectively, $k_{OS} = 3N/4$, the shape and scale parameters are $\alpha = 4.7241$ and $\beta = 0.0446$, respectively; which values correspond to the Ingara database for a spiky and horizontally polarised X-band maritime surveillance radar [28, 29]. At each Monte Carlo run, the scale parameter β is estimated using the maximum likelihood estimator (MLE), which comes out to be the minimum of the ordered samples set, i.e. $\beta = \text{Min}(X_{(i)}) = X_{(1)}$, $i = 1, 2, \ldots, N$ [29, 30]. Note that the shape parameter governs the tail of the Pareto clutter; its values should lie in the interval $(2, \infty)$, i.e. the smaller α is, the spikier the clutter becomes. Fig. 3 shows a set of curves representing simulated probability of error α_0, versus TPI for the given shape parameter and ICR = $-\infty$, 0, 5, 10, 15, 20, 25 dB. Since the PI bears the samples variability, its value allows us to decide whether the background is homogeneous (ICR = $-\infty$). In other words, except the curve relative to the homogeneous case, which is usable, all others just show how α_0 depends upon the ICR value in an interfering background situation. As expected, the larger ICR, the greater α_0. According to a homogeneous background, an order magnitude of the desired $P_{fa} = 10^{-5}$ is $\alpha_0 = 1.05 \times 10^{-5}$, which corresponds to TPI = 0.46. Similarly, Fig. 4 shows the simulated probability of error β_0 versus TMR. According to this curve. Here also, an order magnitude of the desired $P_{fa} = 10^{-5}$ is $\beta_0 = 1.06 \times 10^{-5}$, which is achieved for TMR = 1.44. Once the thresholds levels TPI and TMR are chosen, the switching strategy of Table 2 is used to select the adequate detector.

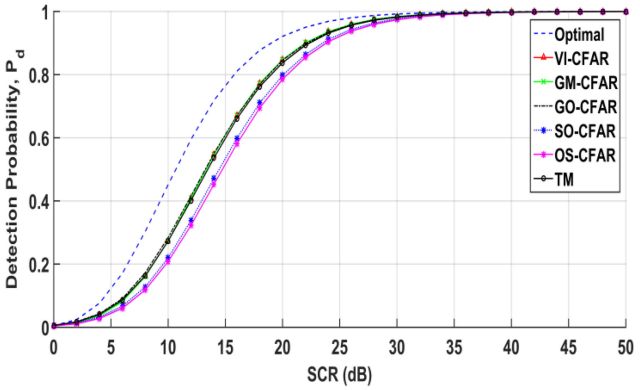

Fig. 5 *Simulated detection probabilities (P_d) of the of the different CFAR detectors versus SCR in a homogeneous environment; for $N = 32$, $P_{fa} = 10^{-5}$, $\alpha = 4.724$, TPI = 0.46 and TMR = 1.44*

4.1 Homogeneous background

According to the obtained values of TPI and TMR, let us assume that the background is homogeneous. Due to the optimal performance of the GM-CFAR detector in such a background, the processor should select it among all those of Table 2. In addition to the detectors cited in Table 2, and for comparison purposes, two more detectors; namely, the smallest of (SO)-CFAR and the order statistic (OS)-CFAR [5, 29, 39] are also analysed along with the fixed threshold detector defined by (20). Fig. 5 shows the detection probability curves versus the signal-to-clutter ratio (SCR) of the different CFAR detectors. It is clear, that the PI-CFAR performs exactly as the GM-CFAR; which agrees with row 1 of Table 2.

$$T_{OPT} = \beta P_{fa}^{-1/\alpha} \quad (20)$$

To illustrate the CFAR property of the PI-CFAR processor, Fig. 6 shows the P_{fa} versus the scale factor τ. Based upon this figure, we can deduce that for $P_{fa} = 8.81 \times 10^{-6}$, the choice of $\tau = 0.4542$ is appropriate.

Fig. 7 shows the resulting PWS. In effect, by means of these curves, we would figure out how the PI-CFAR processor selects effectively the suitable reference window. Specifically, in regard to $PWS_{A\circ B} = 0.9978$, the entire reference window is selected instead of the reference sub-window A or B, whose $PWS_A = PWS_B \simeq 0$. Note that the *SCR* has no effect on these curves.

4.2 Multiple target situations

As a first example of the multiple target situations, Fig. 8 shows the detection curves versus ICR = SCR of the different CFAR detectors in the presence of one interfering target in the reference sub-window A. According to row 3 of Table 2, the PI-CFAR

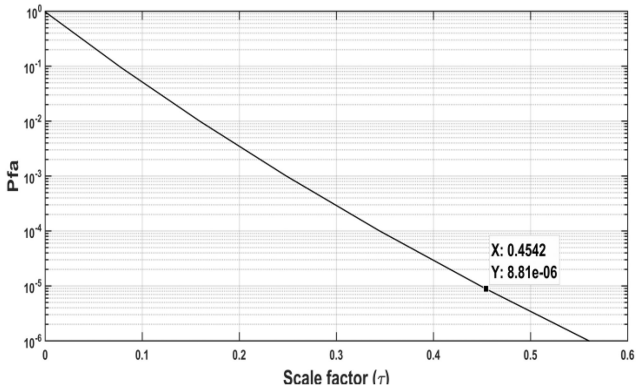

Fig. 6 *Simulated probability of false alarm (P_{fa}) versus scale factor (τ) of the PI-CFAR processor*

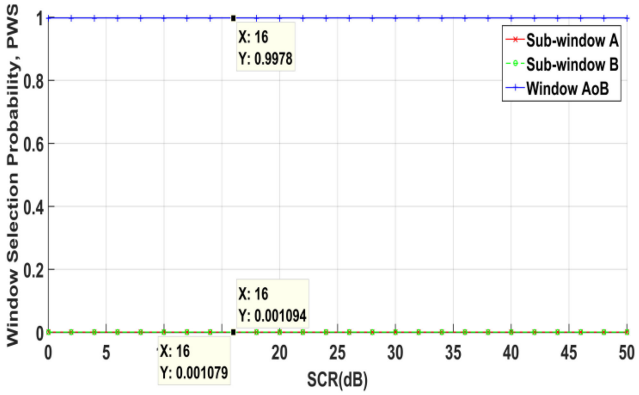

Fig. 7 *Simulated window selection probabilities (PWS) versus SCR, relative to Fig. 5*

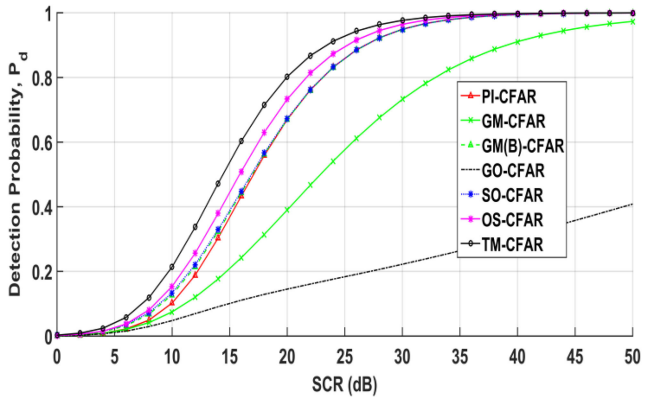

Fig. 8 *Simulated detection probabilities (P_d) of the different CFAR detectors versus SCR in the presence of one interfering target in sub-window A; for $N = 32$, $P_{fa} = 10^{-5}$, $\alpha = 4.7241$, $ICR = SCR$, $TPI = 0.46$ and $TMR = 1.44$*

processor must switch to the GM_B-CFAR detector for all SCR values. However, PWS_A, PWS_B and $PWS_{A\circ B}$ of Fig. 9 show that as long as the *ICR* values are below 9 dB, the PI-CFAR processor is likely to track the $GM_{A\circ B}$-CFAR with a reduced probability value. Then, for larger values of ICR, the PI-CFAR processor switches progressively to the GM_B-CFAR. Note that, in this case, due to the selected sub-window *B*, the PI-CFAR processor switches to neither the TM-CFAR detector nor the OS-CFAR detector. Note that the P_d of the PI-CFAR overlaps that of the SO-CFAR and is slightly better than that of the OS-CFAR detector. To test the robustness of the PI-CFAR processor, we injected an interfering target in sub-window *A* at ICR = 5, 10, 15, 20, 25 and 30 dB, respectively. The resulting values of the ratio of the simulated P_{fa} to the design P_{fa} are reported in Table 3*a*. We notice that the higher the ICR, the better the P_{fa} regulation of the PI-CFAR processor and the GM_B-CFAR detector.

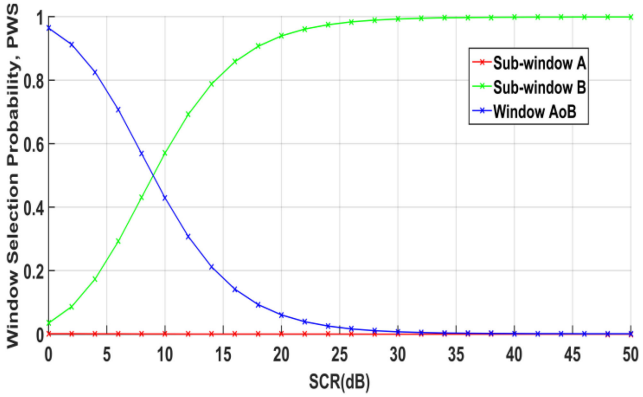

Fig. 9 *Simulated window selection probabilities (PWS) versus SCR, relative to Fig. 8*

As a second example of the multiple target situations, Fig. 10 shows the probability curves versus SCR = ICR of the different CFAR detectors in the presence of two interfering targets, one in each of the sub-windows *A* and *B*. Here, and according to row 5 of Table 2, the PI-CFAR processor must switch to the TM-CFAR detector. In doing this, and as shown in Fig. 11, the PI-CFAR starts by tracking the $GM_{A\circ B}$-CFAR detector for ICR values small <10 dB, and then tracks the TM-CFAR detector until it reaches a complete overlap for ICR values >25 dB. Finally, note that the PI-CFAR processor performs better than the OS-CFAR detector especially for high SCR.

Here also, to test the robustness of the PI-CFAR processor, we injected two interfering targets, one in of the sub-widows *A* and *B* at, respectively, ICR = 5, 10, 15, 20, 25 and 30 dB. The resulting values of the ratio of the simulated P_{fa} to the design P_{fa} are reported in Table 3*b*. We notice that the higher the ICR, the better the P_{fa} regulation of the PI-CFAR processor and the TM-CFAR detector. It is useful to mention that the mean and variance of the background power level under investigation would be very promising to evaluate the robustness of a CFAR detector [40].

Finally, in order to improve the switching algorithm of the PI-CFAR, it is possible to extent the automatic censoring procedure introduced in [37 and references therein] to the TM-CFAR detector with a priori unknown scale parameter and an unknown number of interfering targets and unknown of the clutter position.

4.3 Clutter edge situations

The clutter edge background, generally due to atmospheric and maritime phenomena, is related to an abrupt variation of the clutter power. It is known in the radar literature that the P_{fa} is excessive over the edge area. In this work, we assume a unique clutter transition. In this case, the CUT may be before, on or after the clutter edge. As shown earlier, the first and the third situations are solved by rows 4 and 3, respectively. We are interested with the second situation, i.e. the CUT is exactly on the clutter edge, in which case the two reference sub-windows *A* and *B* are homogeneous. Let us assume that the shape parameters of the low-powered and the high-powered clutter, are, respectively. $\alpha_1 = 4.7241$ and $\alpha_2 = 2/(1 - 10^{(-0.1*\text{CCR})(1-(2/\alpha_1))}) = 2.1115$ for a clutter-to-clutter ratio, CCR = 20 dB. Hence for each clutter power and the same desired probability of error α_0, we should set a TPI value. To this end, Fig. 12 represents the probability of error α_0 versus TPI. The solid line curve illustrates α_0 for the first homogeneous reference sub-window with α_1 as a parameter, and the dashed line curve for the second homogeneous reference sub-window with α_2 as a parameter. For $\alpha_0 \simeq 10^{-5}$, the respective TPI values are clearly shown to be $\text{TPI}_1 = 0.46$ and $\text{TPI}_2 = 0.92$.

Similarly, Fig. 13 illustrates the probability of error β_0 versus TMR; whose curves yield, respectively, $\text{TMR}_1 = 1.44$ and $\text{TMR}_2 = 2.22$.

As a final stage of the PI-CFAR processor performances, we consider the effect of a clutter edge on the false alarm regulation.

Table 3 Regulation of the P_{fa} in a heterogeneous background

Detector	Simulated P_{fa}/design $P_{fa} = 10^{-5}$					
	05 dB	10 dB	15 dB	20 dB	25 dB	*B*
(a) One interfering target in sub-window *A*						
PI-CFAR	0.2399	0.2799	0.3200	0.7798	0.7399	0.7998
GM_B-CFAR	0.4395	0.7194	0.5200	0.8892	0.7501	0.7907
(b) One interfering target in each of sub-windows *A* and *B*						
PI-CFAR	0.0500	0.1300	0.2200	0.3999	0.4898	0.6095
TM-CFAR	0.4699	0.4797	0.5600	0.5297	0.5400	0.6194

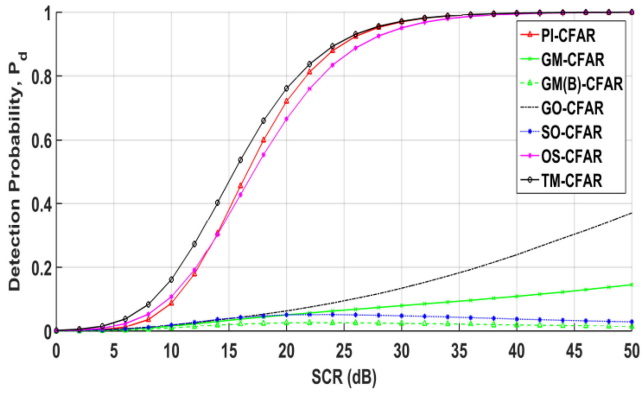

Fig. 10 *Simulated detection probabilities (P_d) of the different CFAR detectors versus SCR in the presence of two interfering targets, one in each of the sub-windows A and B; for N = 32, $P_{fa} = 10^{-5}$, $\alpha = 4.7241$, ICR = SCR, TPI = 0.46 and TMR = 1.44*

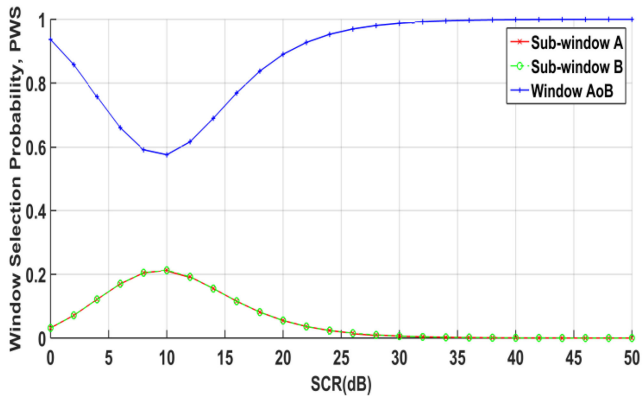

Fig. 11 *Simulated window selection probabilities (PWS) versus SCR, relative to Fig. 10*

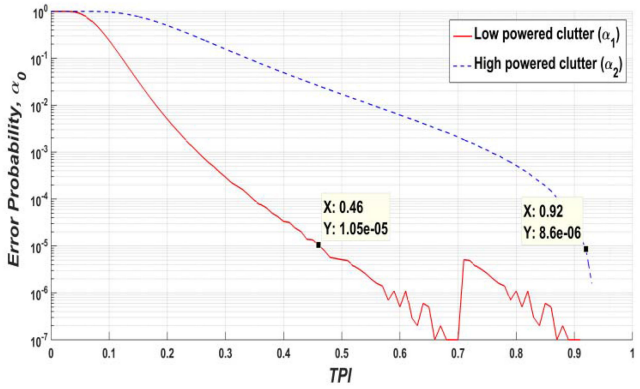

Fig. 12 *Simulated error probabilities (α_0) versus TPI in the case of low and high powered clutters; for N = 32 and $P_{fa} = 10^{-5}$*

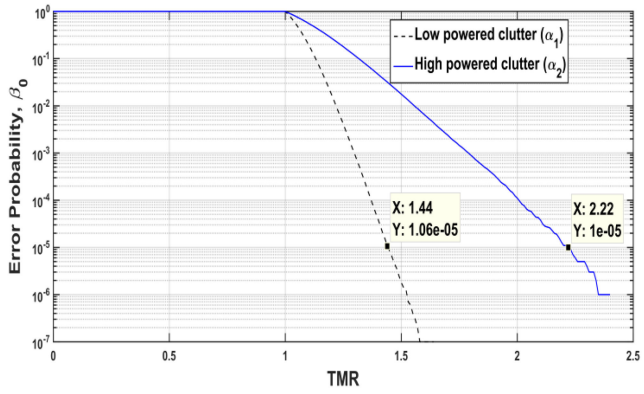

Fig. 13 *Simulated error probabilities (β_0) versus TMR in the case of low and high powered clutters; for N = 32 and $P_{fa} = 10^{-5}$*

To this end, the clutter boundary is modelled as a gradual transition of its power, across the reference cells. This results in a discontinuity between the high-powered clutter and the low-powered clutter within the reference window.

To examine the effects of a clutter edge on the design P_{fa}, we simulate a clutter transition through the generation of two Pareto distributions with two different shape parameters α_1 and α_2. Here, we show the behaviour of the proposed detector performance during clutter transitions, when it progresses from the first reference cell up to the last one, passing through the CUT. That is, the P_{fa} curves are estimated by dynamically varying the clutter edge position in the reference cells. Once exactly half of the clutter reference cells are completely immersed in the high-powered clutter, the CUT is then also considered to be embedded in the higher power clutter. Fig. 14 shows the false alarm rate performance of the different CFAR detectors, versus the number of the high-powered clutter cells at CCR = 20 dB. For the first half of the reference window, we remark that, while the PI-CFAR processor regulates the P_{fa} as good as an even better than the SO- and GM_B-CFAR detectors; all other detectors seem to depart from the design value. When the number of the high-powered clutter cells coincides with the position of the CUT, as expected, the P_{fa} of the PI-CFAR processor shows a sharp discontinuity, but still remains close to that of the GO-CFAR detector until the high-powered clutter covers the entire reference window.

According to the situation where the last high-powered clutter cell overlaps the CUT, Fig. 15 depicts the detection probabilities versus SCR of the different CFAR detectors. Referring to row 2 of Table 2, the PI-CFAR processor should switch to the GO-CFAR detector; which agrees with Fig. 16, where the PWS_A equals to unity for all SCR values, and Fig. 14 in which the P_{fa} of the two detectors are much the same. As the clutter transition progresses, although all detectors do not regulate correctly the P_{fa}, the PI-CFAR processor, along with the GO-CFAR detector, are the only ones which exhibit a good regulation.

4.4 Expected performance of the PI-CFAR processor with real data

This section attempts to show how we could expect the PI-CFAR processor to operate in practice. As the performance of the overall detection scheme critically depends upon the choice of the thresholds TPI and TMR, we recall that, in this paper, they are set to pre-set values whose corresponding probabilities of error α_0 and

β_0 should be limited to an order of magnitude of the design P_{fa}. It is clear that in real-world applications, we are confronted to a priori unknown Pareto clutter parameter. In this case, (10) and (16) become

$$\alpha_0 = \int_0^{+\infty} \Pr(\mathrm{PI} > \mathrm{TPI} \,|\, \mathrm{hH})\, f_{\mathrm{TPI}}(x)\mathrm{d}x \tag{21}$$

where

$$\Pr(\mathrm{PI} > \mathrm{TPI} \,|\, \mathrm{hH}) = \int_{\mathrm{TPI}}^{+\infty} f_{\mathrm{PI}}(x)\mathrm{d}x \tag{22}$$

Similarly

$$\begin{aligned}\beta_0 = &\int_0^{+\infty} f_{\mathrm{TMR}}(x)\mathrm{d}x \\ &- \int_0^{+\infty} \Pr\left(\mathrm{TMR}^{-1} \le \mathrm{LGMR} \le \mathrm{TMR} \,|\, \mathrm{hH}\right) f_{\mathrm{TMR}}(x)\mathrm{d}x\end{aligned} \tag{23}$$

where

$$\Pr\left(\mathrm{TMR}^{-1} \le \mathrm{LGMR} \le \mathrm{TMR} \,|\, \mathrm{hH}\right) = \int_{\mathrm{TMR}^{-1}}^{\mathrm{TMR}} f_{\mathrm{LGMR}}(x)\mathrm{d}x \tag{24}$$

Now, if we consider adaptive thresholds TPI and TMR, we should evaluate, through Monte Carlo simulations, (21) and (23). To do it analytically, we should, first evaluate the PDFs $f_{\mathrm{PI}}(x)$ and $f_{\mathrm{LGMR}}(x)$ of the PI and LGMR given by (7) and (14), respectively, and the PDFs $f_{\mathrm{TPI}}(x)$ and $f_{\mathrm{TMR}}(x)$ from some thresholds whose forms are to be determined; and then solve for α_0 and β_0 the integrals of (21) and (23), respectively. In this way, the thresholds TPI and TMR would adapt automatically to the changes of the Pareto background.

Another issue that may arise in practice is the fact that real clutter data contains values arbitrarily close to zero, so the sample minimum, i.e. $\mathrm{Min}(X_{(i)}) = X_{(1)}$, $i = 1, 2, \ldots, N$ cannot be used to estimate the scale parameter β. In which case, as it is stated in [40], we should first, for each radar set, estimate the scale parameter using the ML estimator. Then, scale the data by β. This normalises the dataset, producing an unbiased estimator. The real data are thus pre-processed by censoring any returns smaller than the scale parameter β. This yields reduced sample set sizes, but provides more valid outcomes.

Finally, it has been shown in [41] that although the detectors proposed in [29, 30], upon which the PI-CFAR processor is built, attain the CFAR property without a priori knowledge of the scale parameter β; i.e. they assumed that the clutter sample are drawn from a Pareto type I law, and therefore do not contain any sample smaller than β. Nevertheless, this assumption is not valid in practice; in this respect the Pareto type II law with support beginning at zero, is a better model for the Pareto clutter. Unfortunately, the authors showed that there is not any CFAR property with respect to β. According to this result, we may still compare the overall performance of the PI-CFAR processor based on the data pre-processing steps given in [42].

5 Conclusion

In this work, we addressed the problem of automatic target detection in a heterogeneous Pareto background. In doing this, we developed the PI-CFAR. Assuming a non-stationary Pareto background with the presence or not of any clutter edge or interfering targets, the PI and the LGMR statistic tests were concomitantly used to allow the proposed processor to switch dynamically to the appropriate detector; i.e. the GM-CFAR, the GO-CFAR or the TM-CFAR, whose scale parameter is a priori unknown. Depending upon the window selection probability (PWS), the background level is estimated according to the preselected detector. The detection performances of the proposed

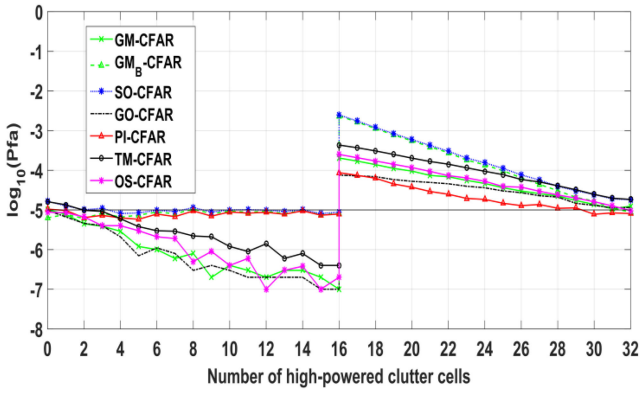

Fig. 14 *Simulated probability of False Alarm (P_{fa}) regulation of the different CFAR detectors versus the number of high-powered clutter cells at CCR = 20 dB; for N = 32, $P_{fa} = 10^{-5}$, $\alpha_1 = 4.7241, \alpha_2 = 2.1115$, $TPI_1 = 0.46$, $TPI_2 = 0.92$, $TMR_1 = 1.44$ and $TMR_2 = 2.22$*

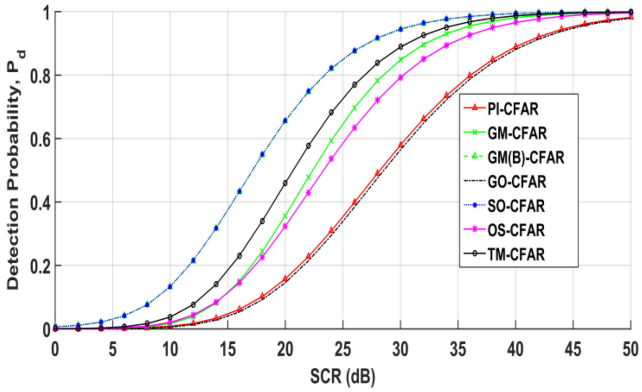

Fig. 15 *Simulated detection probabilities (P_d) of the different CFAR detectors versus SCR in the presence of a clutter edge for which the last high-powered clutter cell overlaps the CUT at CCR = 20 dB; for N = 32, $P_{fa} = 10^{-5}$, $\alpha_1 = 4.7241$, $\alpha_2 = 2.1115$, $TPI_1 = 0.46$ and $TPI_2 = 0.92$, $TMR_1 = 1.44$, $TMR_2 = 2.22$*

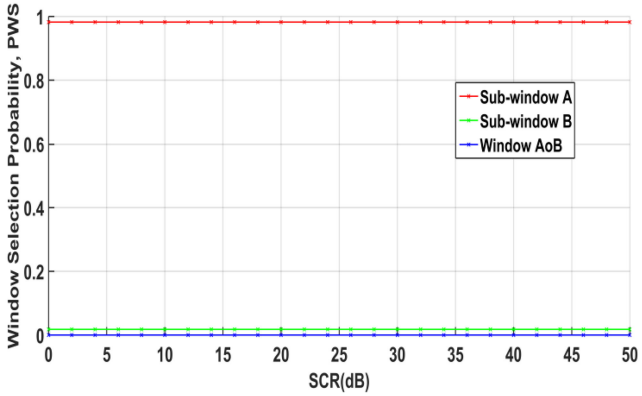

Fig. 16 *Simulated window selection probabilities (PWS) versus SCR, relative to Fig. 15*

processor were assessed via extensive Monte Carlo simulations. As expected, for a homogeneous Pareto clutter, the PI-CFAR processor overlaps the GM$_{A\circ B}$-CFAR detector, for a unique interfering target, it tracks the GM$_B$-CFAR or equivalently the SO-CFAR detector, and for two interfering targets, one in each of the reference sub-windows; it tracks the TM-CFAR detector. For a clutter edge situation, we showed that the PI-CFAR processor performs a fair regulation of the false alarm rate and tracks the GO-CFAR detector when the last high-powered clutter cell joins the CUT. As an overall conclusion, we may think of the PI-CFAR processor as an effective non-Gaussian background-dependent detector. In other words, we showed that the PI statistic is a good

substitute for the VI statistic, which happens to be a handy discriminator in a Gaussian background only. Finally, as an ultimate opening for future works, we may consider TPI and TMR as adaptive thresholds.

6 Acknowledgments

The authors were grateful to the reviewers and the field editor for their constructive comments which helped to enhance the quality of the paper.

7 References

[1] Barkat, M.: '*Signal detection and estimation*' (Artech House, Norwood, MA, 2005, 2nd edn)

[2] Skolnik, M.I.: '*Introduction to radar system*' (McGraw-Hill, New York, 1981, 2nd edn)

[3] Rickard, J.T., Dillard, G.M.: 'Adaptive detection algorithms for multiple target situations', *IEEE Trans.*, 1977, **AES-13**, (4), pp. 338–343

[4] Himonas, S.D., Barkat, M.: 'Automatic censored CFAR detection for nonhomogeneous backgrounds', *IEEE Trans. Aerosp. Electron. Syst.*, 1992, **AES-28**, (1), pp. 286–304

[5] Gandhi, P.P., Kassam, S.A.: 'Analysis of CFAR processors in nonhomogeneous background', *IEEE Trans.*, 1988, **AES-24**, (4), pp. 427–445

[6] Srinivasan, R.: '*Importance sampling: applications in communications and detection*' (Springer, Berlin, Germany, 2002)

[7] Anastassopoulos, V., Lampropoulos, G.: 'A new and robust CFAR detection algorithm', *IEEE Trans. Aerosp. Electron. Syst.*, 1992, **28**, (2), pp. 420–427

[8] Barkat, M., Himonas, S.D., Varshney, P.K.: 'CFAR detection for multiple target situations', *IEE Proc. F, Radar Signal Process.*, 1989, **136**, (5), pp. 193–209

[9] Smith, M.E., Varshney, P.K.: 'Intelligent CFAR processor based on data variability', *IEEE Trans. Aerosp. Electron. Syst.*, 2000, **AES-36**, pp. 837–847

[10] Hammoudi, Z., Soltani, F.: 'Distributed IVI-CFAR detection in nonhomogeneous backgrounds', *Signal Process.*, 2004, **84**, (7), pp. 1231–1237

[11] Farrouki, A., Barkat, M.: 'Automatic censoring CFAR detector based on ordered data variability for nonhomogeneous backgrounds', *IEE Proc., Radar Sonar Navig.*, 2005, **152**, (1), pp. 43–51

[12] Cao, T.T.V.: 'Constant false alarm rate algorithm based upon test cell information', *IET Radar Sonar Navig.*, 2008, **2**, (3), pp. 200–213

[13] Zhang, R., Sheng, W., Ma, X.: 'Improved switching CFAR detector for non-homogeneous backgrounds', *Signal Process*; Elsevier, 2012, **93**, (1), pp. 35–48

[14] Tabet, L., Soltani, F.: 'A generalized switching CFAR processor based on test cell statistics', *Signal. Image. Video. Process.*, 2009, **3**, (3), pp. 265–273

[15] Finn, M.M., Johnson, R.S.: 'Adaptive detection mode with threshold control as a function of spatially sampled clutter level estimates', *RCA Rev.*, 1968, **30**, pp. 414–465

[16] Trunk, G.V.: ''Range resolution of targets using automatic detectors'', *IEEE Trans. Aerosp. Electron. Syst.*, 1978, **14**, (5), pp. 750–755

[17] Hansen, G.V., Sawyers, J.H.: 'Detectability loss due to greatest-of selection in a cell averaging CFAR', *IEEE Trans. Aerosp. Electron. Syst.*, 1980, **16**, pp. 115–118

[18] Trunk, G.V.: 'Radar properties of non-Rayleigh sea clutter', *IEEE Trans. Aerosp. Electron. Syst.*, 1972, **8**, (2), pp. 196–204

[19] Pourmottaghi, A., Taban, M.R., Gazor, S.: 'A CFAR detector in a non-homogenous Weibull clutter', *IEEE Trans. Aerosp. Electron. Syst.*, 2012, **48**, (2), pp. 1747–1758

[20] Ward, K.D.: 'Compound representation of high resolution sea clutter', *Electron. Lett.*, 1981, **17**, (16), pp. 561–563

[21] Almarshad, M.N., Alshebeili, S.A., Barkat, M.: 'A forward automatic censored cell-averaging detector for multiple target situations in log-normal clutter', *Trans. Eng. Comput. Technol.*, 2006, **17**, pp. 281–286

[22] Almarshad, M.N., Barkat, M., Alshebeili, S.A.: 'A Monte Carlo simulation for two novel automatic censoring techniques of radar interfering targets in log-normal clutter', *Signal Process.*, 2008, **88**, (3), pp. 719–732

[23] Weber, P., Haykin, S.: 'Ordered statistic CFAR processing for two-parameter distributions with variable skewness', *IEEE Trans. Aerosp. Electron. Syst.*, 1985, **AES-21**, (6), pp. 819–821

[24] Chabbi, S., Laroussi, T., Barkat, M.: 'Performance analysis of dual automatic censoring and detection in heterogeneous Weibull clutter: a comparison through extensive simulations', *Signal Process.*, 2013, **93**, (11), pp. 2879–2893

[25] Weinberg, G.V.: 'Formulation of a generalized switching CFAR with application to X-band maritime surveillance radar', *Springerplus*, 2015, **4**, p. 574

[26] Weinberg, G.V.: 'Geometric mean switching constant false alarm rate detector', *Digit. Signal Process.*, 2017, **69**, pp. 1–10

[27] Mehanaoui, A., Laroussi, T., Attalah, M.A*., et al.*: 'An EVI-ASD-CFAR processor in Pareto background and multiple target situations'. IEEE 7th Int. SETIT'16 Conf., Tunisia, Hammamet, 2016

[28] Weinberg, G.V.: 'Constant false alarm rate detections for Pareto clutter models', *IET Radar Sonar Navig.*, 2013, **7**, pp. 153–163

[29] Weinberg, G.V.: 'On the construction of CFAR decision rules via transformations', *IEEE Trans. Geosci. Remote Sens.*, 2017, **55**, pp. 1140–1146

[30] Weinberg, G.V.: 'Trimmed geometric mean order statistic CFAR detector for Pareto distributed clutter', *Signal Image Video Process.*, 2018, **12**, (4), pp. 651–657

[31] Farshchian, M., Posner, F.L.: 'The Pareto distribution for low grazing angle and high resolution X-band sea clutter'. IEEE Radar Conf., Washington, DC, USA, 2010, pp. 789–793

[32] Weinberg, G.V.: 'Constant false alarm rate detection in Pareto distributed clutter: further results and optimality issues', *Contemp. Eng. Sci.*, 2014, **7**, (6), pp. 231–261

[33] Arnold, B.C.: '*Pareto distributions*' (Chapman & Hall/CRC Monographs on Statistics & Applied Probability, Boca Raton, FL, USA, 2015, 2nd edn)

[34] Eliazar, I., Sokolov, I.M.: 'Measuring statistical heterogeneity: the Pietra index', *Physica A*, 2010, **389**, (1), pp. 117–125

[35] Eliazar, I.: 'The Pietra term structures of financial assets', *Physica A*, 2011, **390**, pp. 699–706

[36] Sarabia, J.M., Jordá, V.: 'Explicit expressions of the Pietra index for the generalized function for the size distribution of income', *Physica A*, 2014, **416**, pp. 582–595

[37] Mehanaoui, A., Laroussi, T., Chabbi, S*., et al.*: 'Trimmed mean based automatic censoring and detection in Pareto background'. Proc. IEEE 4th Int. Conf. Elect. Eng., Boumerdes, Algeria, 2015, pp. 1–4

[38] Ravid, R., Levanon, N.: 'Maximum-likelihood CFAR for Weibull background', *IEE Proc. F*, 1992, **139**, (3), pp. 256–264

[39] Rohling, H.: 'Radar CFAR thresholding in clutter and multiple target situations', *IEEE Trans. Aerosp. Electron. Syst.*, 1983, **AES-19**, (4), pp. 608–621

[40] Zhou, W., Xie, J., Zhang, B*., et al.*: 'Maximum likelihood detector in gamma-distributed sea clutter', *IEEE Geosci. Remote Sens. Lett.*, 2018, **15**, (11), pp. 1705–1709

[41] Rosenberg, L., Weinberg, G.V.: 'Performance analysis of Pareto CFAR detectors'. Int. Conf. Radar Systems, Belfast, UK, October 2017, pp. 1–6

[42] Alexopoulos, A., Weinberg, G.V.: 'Fractional order Pareto distributions with application to X-band maritime radar clutter', *IET RSN*, 2015, **9**, (7), pp. 817–826